

4.5 kV-Fast-Diodes with Expanded SOA Using a Multi-Energy Proton Lifetime Control Technique

O. Humbel, N. Galster, F. Bauer, W. Fichtner

ISPSD, May 1999, Toronto, Canada

Copyright © [1999] IEEE. Reprinted from the International Symposium on Power Semiconductor Devices and ICs.

This material is posted here with permission of the IEEE. Such permission of the IEEE does not in any way imply IEEE endorsement of any of ABB Switzerland Ltd, Semiconductors's products or services. Internal or personal use of this material is permitted. However, permission to reprint/republish this material for advertising or promotional purposes or for creating new collective works for resale or redistribution must be obtained from the IEEE by writing to pubs-permissions@ieee.org.

4.5 kV-Fast-Diodes with Expanded SOA Using a Multi-Energy Proton Lifetime Control Technique

O. Humbel ★, N. Galster ■, F. Bauer ■, W. Fichtner ★

■ ABB Semiconductors Lenzburg, Switzerland
 Phone: +41/62 888 63 79; Fax: +41/62 888 63 05; E-Mail: galster@abbsem.ch

★ Integrated Systems Laboratory, ETH Zürich, Switzerland
 Phone: +41/632 60 95; Fax: +41/632 11 94; E-Mail: humbel@iis.ee.ethz.ch

Abstract: This paper presents a 4.5 kV diode fabricated using a new ion irradiation technique whereby electrons are replaced by protons in a second irradiation step. The second proton peak is located close to the middle of the n-base. Compared to the combined ion-electron irradiation, diodes with a double proton peak show a smaller maximum reverse-recovery current and a much smoother tail current behavior. The new device has an excellent ruggedness, being able to withstand a peak power of 1 MW/cm².

I. INTRODUCTION

With increasing demands for higher switching frequencies, new power switches such as the Hard Driven GTO [1] - or IGCT - and the IGBT require improved diode concepts. Snubberless conditions in these applications are gaining ground, imposing switching transients at very high di/dt and dv/dt values. This leads to new challenges in diode development. Besides the standard criteria of low static and dynamic losses, soft recovery under all application conditions (in particular at low current density and high line voltage) and low reverse-recovery current, the need for a large SOA (Safe Operating Area) has become most important. The optimum diode design depends on the specific application conditions. In the following, the new 4.5 kV diode is investigated in two different applications (clamped inductive and resistive switching), computer simulations employing lifetime profiles will be compared to the test results.

II. COMMUTATION CONDITIONS

In order to optimize the behavior of diodes during turn-off, the circuit needs to be taken into consideration in particular with respect to “inductive” and “resistive” switching. Fig. 1 shows a clamped inductive circuit with a “perfect switch”, which results in a linear di/dt determined by the external inductance L. This differs essentially from the resistive mode of commutation (Fig. 2). Here the turn-off is controlled by an active switch, which switches progressively over a defined period of time. This means that the di/dt is determined by R_τ (time-dependant resistance of the switch) rather than by the stray inductance

L_S. This type of circuit is realized for Undeland snubbers where the active switch

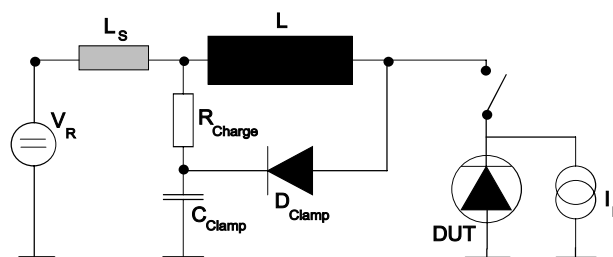


Fig. 1 Snubberless, clamped inductive switching circuit

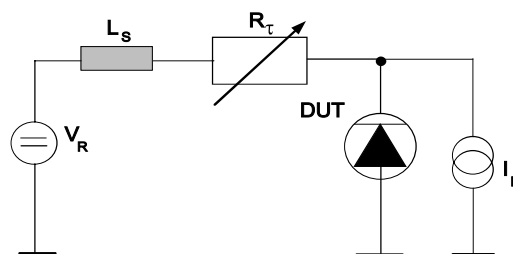


Fig. 2 Snubberless Undeland/Mc Murray snubber diode, resistive switching circuit

is typically a GTO or in freewheeling diodes circuits where the active switch is an IGBT. The differences in the stress that the diode experiences will be explained in chapter IV.

III. MULTI-ENERGY PROTON LIFETIME CONTROL

The design concepts for diode optimization include basically the variation of emitter efficiency and lifetime control. Local lifetime control has proven to be very successful and is realized by either heavy metal doping or by exposure to ion beams (protons or α particles), in addition to electron irradiation [2,5]. Ion irradiation is intended to reduce anode emitter efficiency and hence the plasma density close to the anode thus leading to lower maximum reverse current and a “softer” recovery behavior. Due to the carrier lifetime reduction both in the n-base and

cathode area of the diode, electron irradiation yields a tail-current phase free from heavy impact ionization caused by dynamic avalanche, but the possibilities of further tailoring the plasma distribution in the diode are very limited [3].

In this paper we present the results of a new irradiation technique where electron irradiation is replaced by proton irradiation in a second step. The second proton peak is located close to the middle of the n-base (Fig. 3). This results in a favorable carrier distribution with lower concentration at the anode and higher concentration at the cathode side as compared to a device with combined proton and electron irradiation. (Fig. 4).

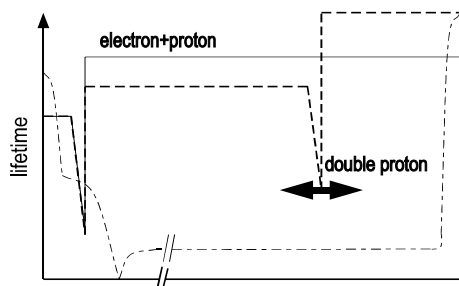


Fig. 3. Doping (dot dashed) and lifetime profiles of the combined p^+/e^- (solid) and the double-proton irradiated (dashed) diode

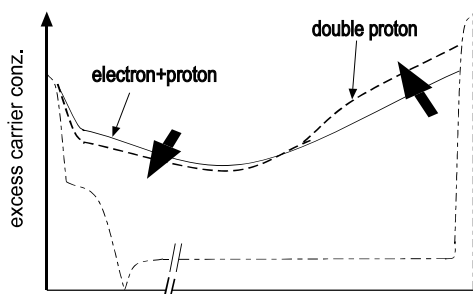


Fig. 4. Doping profile (dot dashed) and on-state plasma distributions of the conventionally (solid) and the double-proton irradiated (dashed) diode

IV. DEVICE SIMULATION

For the two different applications mentioned above, a 1-dimensional computer simulation employing lifetime profiles will be compared to the test results (Fig. 6 and Fig. 13 are used to explain the physical processes).

An initial trap distribution and related capture cross-sections were taken from work carried out previously [7] and the resulting excess carrier lifetime was calculated and implemented into the device simulator DESSIS [4].

A linear approximation for different proton doses and energies turned out to be acceptable. The physical models of the simulator were optimized for good agreement between the measurements under resistive, snubberless conditions and the simulations (Fig. 6).

The virtual devices obtained by this procedure (e.g. same doping- and lifetime profiles and same physical models) were then implemented in the clamped inductive topology

(Fig. 2) and showed good agreement with the measured data without further calibration (Fig. 13).

V. MEASURED AND SIMULATED REVERSE-RECOVERY CHARACTERISTICS

A. Resistive, Snubberless Condition

In this mode the commutation di/dt is controlled by the active switch, which in our case is a GTO, and typically is in the range of 50 to 100 $A/\mu\text{scm}^2$ at zero current crossing, accelerating towards the max. reverse current I_{RR} [2]. Snap-off of the diode current is most likely to occur at low forward current densities ($1A/\text{cm}^2 \dots 3 A/\text{cm}^2$) and high DC-voltages and is more likely to impose problems on the neighboring circuitry than on the device itself. Dynamic avalanche, on the contrary occurs at high forward current and high voltage and may result in the destruction of the device itself. The maximum power a diode can withstand during turn off gives us a measure of the ruggedness (SOA) of the device.

In Fig. 5, the reverse-recovery waveforms of two diodes with the same on-state voltage drop of 7.1V but different lifetime profiles are compared at $420 A/\text{cm}^2$.

The double-proton irradiated diode has a soft recovery, i.e. a smooth decay of the diode current without abrupt changes, even at forward currents as low as $1A/\text{cm}^2$ and at a line voltage as high as 3.6 kV. This diode also has a smaller maximum reverse-recovery current and consequently a lower maximum peak power density. The conventional diode with combined e^-/p^+ irradiation by contrast shows a greater reverse peak current and significant snap-off.

To understand the physical processes of the reverse-recovery of devices with different lifetime profiles, the simulation described in chapter IV was employed.

The charge carriers in a diode are extracted through the anode and cathode immediately after the voltage is reversed. As a consequence, in the device with combined electron and proton irradiation, a space charge region is formed not only across the pn-junction, but also across the n^+/n^- -junction under the applied recovery conditions.

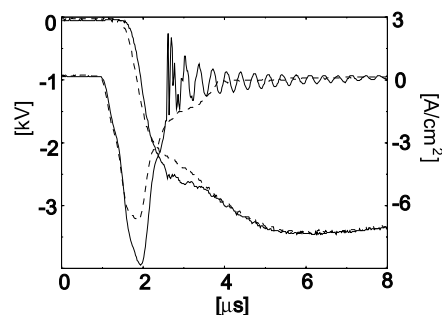


Fig. 5. Reverse-recovery waveforms of the double-proton irradiated (dashed) diode compared to the waveform of a combined p^+/e^- -irradiated diode.

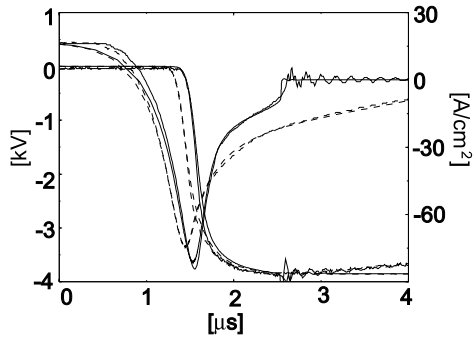


Fig. 6. Simulated and measured reverse-recovery characteristics of a double-proton irradiated (dashed) and p^+/e^- -irradiated (solid) device.

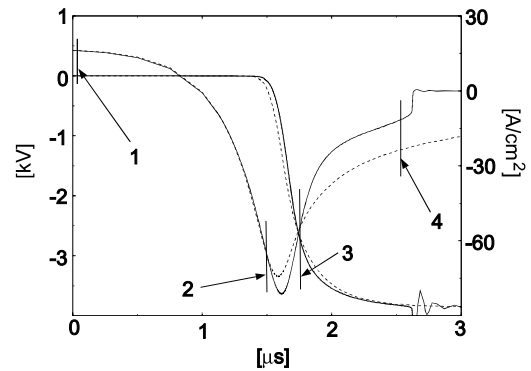


Fig. 8. Simulated reverse-recovery characteristics of a double proton irradiated (dashed) and p^+/e^- -irradiated (solid) device $I_F=16A/cm^2$, $U_{DC}=4kV$ (same as in Fig.6).

This results in a virtual reduction of the usable base-region (Fig. 7) and to snap-off of the reverse current at the moment when the two space-charge regions meet at voltages lower than the static punch-through voltage. Due to the lower recombination rate and consequently stronger diffusion of holes into the base-region of the device with profiled lifetime as obtained by double-energy proton irradiation, the slope of the electric field is steeper compared to that of the device with a lifetime profile as obtained by single-energy proton irradiation combined with electron irradiation. This in turn delays also the "punch through" of the space-charge region towards the cathode stopping layer and therefore supports "soft recovery" even up to voltages beyond the static punch-through voltage.

To increase the applied voltage of a proper device, the behavior of the electric field and the carrier distribution during recovery are of fundamental interest.

Fig. 7 illustrates the simulated electrical field of the double- p^+ irradiated diode compared to that of the $p^+ \& e^-$ irradiated device. Fig.9 compares the hole distributions during reverse-recovery as shown in Fig. 8.

For the comparably snappy recovery of the $p^+ \& e^-$ irradiated diode, one can see an additional electric field on the cathode side.

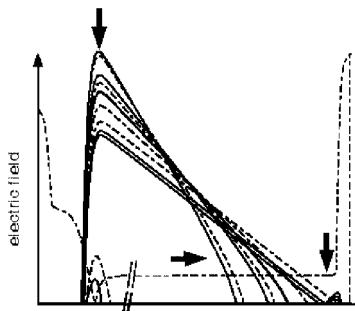


Fig. 7. The simulated field distribution of a double-proton irradiated (dashed) diode compared to a conventionally irradiated (solid) device during turn-off.

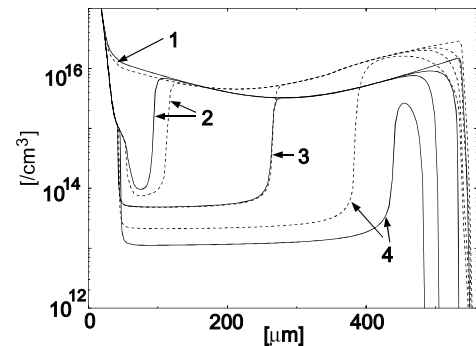


Fig. 9. Simulated hole distribution at 4 points of time during the reverse-recovery shown in Fig. 8

There is almost no voltage drop possible across this second space-charge region because of the majority-carrier influenced electric field. In contrast, the field on the anode side is governed by the *minority* carriers.

The voltage rise over the double-irradiated device leads to a comparatively lower maximum electric field and to a faster propagation of the depletion region into the n-base up until point 2 (Fig. 9) as compared to the $p^+ \& e^-$ -irradiated diode. Towards the end of the recovery phase the situation however changes.

The different speeds at which the depletion region is built up are also illustrated in Fig. 9. Here the depletion speed at low voltage is much higher (Fig. 9, Points 1 & 2) in the double-proton irradiated device than in the electron/proton irradiated diode which results in a reduced I_{rr} . However, at high voltage, toward the end of the recovery phase (Fig. 9, Points 3 & 4), the space-charge region moves more slowly in the double-irradiated diode, resulting in a softer recovery. This is a result of the higher amount of carriers close to the cathode in the double- p^+ irradiated device.

The improved peak power handling capability of the double-proton irradiated diode is illustrated in Fig. 10. This shows the diode turn-off waveforms of a double-proton irradiated diode at a forward current of $90 A/cm^2$ and a reverse supply-voltage of $3.2 kV$ which results in a peak power dissipation of $1MW/cm^2$ without destruction of the device.

This is a significantly improved capability as compared to previously tested devices with either electron or combined p^+/e^- -irradiation, where the destruction was observed at peak power levels between 150 and 250 kW/cm² [2].

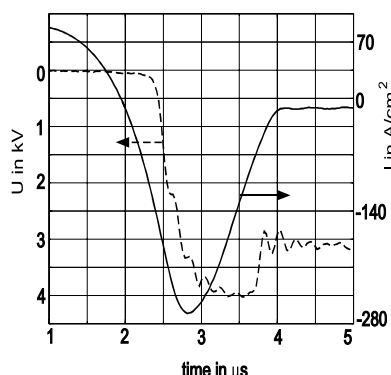


Fig. 10. Reverse-recovery of a double-proton irradiated diode: $I_F = 90 \text{ A/cm}^2$; $U_{DC} = 3.2 \text{ kV}$; 125°C which leads to a peak power of 1 MW/cm^2 ($I_{rr} \approx 270 \text{ A/cm}^2$ and $U_{max} \approx 4 \text{ kV}$)

B. Clamped Inductive Commutation

This type of operation is of growing importance in Voltage Source Inverters (VSI) where snubberless IGBTs demand equally un-snubbed FWDs and Neutral Point Clamping (NPC) diodes (multi-level inverters). The voltage across the diode increases to its maximal value while the full reverse current flows. Diode current I_{RR} from current source L (Fig. 1) cannot decline until $V_{cl} = V_R$ is reached. Once the clamp becomes effective, the recovery current declines while the diode voltage remains constant [2].

Fig. 11 shows the waveforms of p^+ & e^- -irradiated diode during clamped, inductive turn-off at 2.8 kV supply voltage. The diode exhibits snappy behavior at a forward current of 6 A/cm². In contrast the diode with double-proton irradiation (Fig. 12) shows the on-set of snap-off at a clamp voltage of between 3.8 and 4 kV for the same forward current. This is an increase of more than 1000 V for a 4.5 kV diode.

The peak power dissipated by the diode during turn-off under such conditions may be approximated by multiplying peak reverse-recovery current with clamp voltage: $V_R \cdot I_{RR} \approx 90 \text{ kW/cm}^2$.

The circuit as depicted in Fig. 2 was implemented in the device simulator and the same virtual device structure as investigated under resistive, snubberless conditions was compared to the measured waveforms (Fig. 13).

For both simulation and measurement, the conditions are: $I_F = 6 \text{ A/cm}^2$, $L = 1000 \mu\text{H}$ and $V_R = 2900 \text{ V}$, $di/dt = 50 \text{ A}/\mu\text{s cm}^{-2}$. The test and simulation circuit is shown in Fig. 1. The simulation result can be seen to be in excellent agreement with the measurement.

C. Comparison of Commutation Modes

With the help of numerical device investigations, the physical stresses on the DUT, especially the differences between those of inductive, clamped and resistive commutation were analyzed.

Fig. 14 shows the different recovery processes for a double-proton irradiated device with an initial current density of 6 A/cm² and a clamp-voltage of 3kV.

An obvious difference between commutation modes lies in the value of the voltage occurring at the peak of reverse-recovery current. For inductive, clamped commutation, maximum reverse-recovery current and maximum voltage occur simultaneously. The peak power under comparable switching conditions is always higher as compared to the resistive-switching mode.

In this situation, the full clamp voltage is applied over a reduced space-charge region. Due to this lower field-expansion into the base-region of the device, the slope of the electric field is steeper as compared to that of the resistive circuit conditions.

The different field distributions are shown in Fig. 15 for both commutation modes, at the points where voltage starts to rise (point 1), where DC-voltage is reached (point 2) and at zero current (point 3).

Additionally the extension of the space-charge region during the recovery phase is plotted (Fig. 14).

Concerning the snappiness criteria, the design rules are similar to the those for the resistive mode. The increased excess carrier concentration at the cathode prevents the formation of a second electric there, which results in a smooth reverse-recovery current.

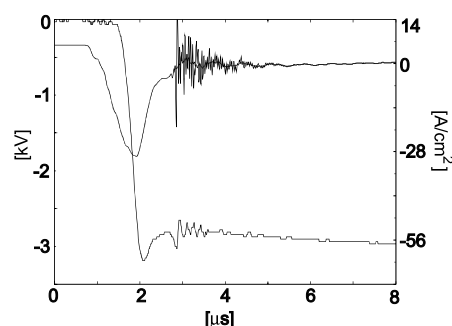


Fig. 11. Measured reverse-recovery of a conventional irradiated device in a clamped, inductive switching mode with a snappy recovery at $U_{clamp} = 2.8 \text{ kV}$, $I_F = 6 \text{ A/cm}^2$

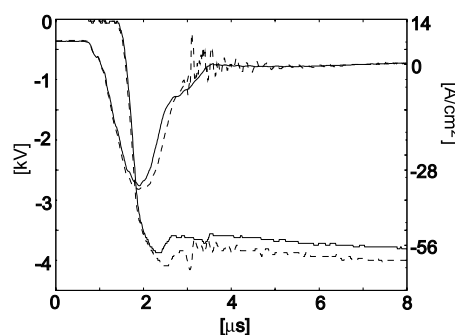


Fig. 12. Measured reverse-recovery of a double-proton irradiated device in a clamped, inductive switching mode ($U_{clamp} = 3.8$ and 3.9 kV , $I_F = 6 \text{ A/cm}^2$)

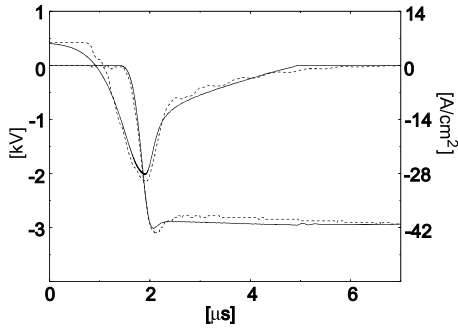


Fig. 13. Measured (*dotted*) and simulated (*solid*) reverse-recovery characteristic of a double-proton irradiated device in a clamped inductive switching mode ($U_{\text{clamp}} = 2.9 \text{ kV}$, $I_F = 6 \text{ A/cm}^2$)

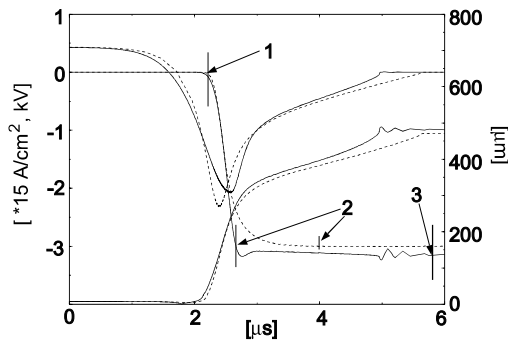


Fig. 14. Recovery of a double-proton irradiated diode in resistive (*dashed*) and inductive, clamped (*solid*) circuit ($U_{\text{DC}}/U_{\text{clamp}} = 3 \text{ kV}$, $I_F = 6 \text{ A/cm}^2$) and the corresponding width of the space charge region

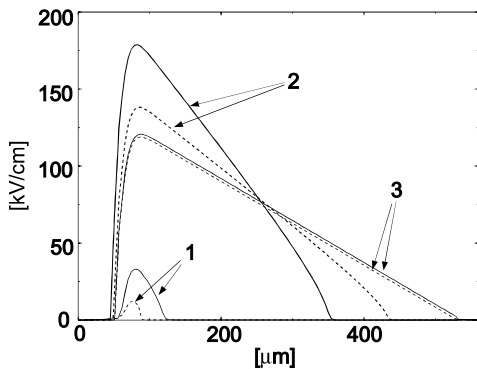


Fig. 15. Electric field during the recovery of a double-proton irradiated diode in a resistive (*dashed*) and an inductive clamped (*solid*) circuit at the 3 points mentioned

V. CONCLUSION

It has been verified by testing that multiple-proton irradiation techniques applied to diodes as already suggested in [2] brings a significantly improved diode performance with respect to snappiness under both resistive and inductive switching conditions in comparison to combined electron and proton irradiation.

In addition, the SOA of the double-proton irradiated device shows an increase - by a factor of 2 to 4 - in power handling capability as compared to devices with combined e^-p^+ -irradiation.

We have shown that a 1-dimensional computer simulation employing lifetime profiles can be used to model device performance and to explain the physical processes of a diode undergoing turn-off. The excellent agreement of simulated and tested turn-off characteristics allows reliable prediction of device performance and avoids laborious experimentation.

ACKNOWLEDGMENT

The authors wish to thank Stefan Müller and Kurt Haas of the Q&R department and Mark Frecker and Hans Vetsch of the Production Test department of ABB Semiconductors for their help in device testing.

REFERENCES

[1] H. Grüning, B. Oedegard, J. Rees, A. Weber, E. Carroll and S. Eicher, "High-power hard-driven GTO module for 4.5 kV/3 kA snubberless operation", PCIM 96 Europe, p.169-183, 1996

[2] N. Galster, M. Frecker, E. Carroll, J. Vobecky and P. Hazdra, "Application-Specific Fast-Recovery Diode: Design and Performance", Proc. PCIM, Tokyo 98, p. 69, 1997

[3] J. Vobecky, and P. Hazdra, "Future Trends in Local Lifetime Control", Proc. ISPSD 96, p.161, 1996

[4] R. Escoffier, W. Fichtner, D. Fokkema, E. Lyumkis, O. Penzin, B. Polsky, A. Schenk and B. Schmithüsen, "DESSIS 5.0 Manual", ISE Integrated Systems Engineering AG, CH - Zürich, 1996

[5] J. Vobecky, P. Hazdra, N. Galster, E. Carroll, "Free-wheeling diodes with improved reverse-recovery by combined electron and proton irradiation", Proc. PEMC'98, pp.1-22 - 1-25

[6] J. Vobecky and P. Hazdra, "Simulation of power diodes", Internal Report, Prague 1996